12 Wang, W. C., Yung, Y. L., Lacis, A. A., Mo, T. & Hansen, J. E. *Science* **194**, 685–690 (1976).
13. Deal, P. L., Keyser, G. L., Fisher, B. D. & Crabill, N. L. *AIAA Pap.* 81-2412 (1981).
14. Fisher, B. D., Keyser, G. L. & Deal, P. L. *NASA Tech. Pap.* **2087** (1982).
15 Bates, D. R. & Hays, P. B. *Planet. Space. Sci.* **15**, 189–196 (1967).
16. Zipf, E. C. *Nature* **287**, 523–524 (1980).
17. Zipf, E. C. & Prasad, S. S. *Nature* **287**, 525–526 (1980).
18. Prasad, S. S. *Nature* **289**, 386–388 (1981).
19. Prasad, S. S. & Zipf, E. C. *Nature* **291**, 564–566 (1981).
20. Zipf, E. C. & Prasad, S. S. *Nature* **295**, 133–135 (1982).
21. Parks, G. K., Mauk, B. H., Spiger, R. & Chin, *Geophys. Res. Lett.* **8**, 1176–1179 (1981).

Positive ion composition measurements and acetonitrile in the upper stratosphere

E. Arijs, D. Nevejans & J. Ingels

Belgian Institute for Space Aeromony, Ringlaan 3, B-1180 Brussels, Belgium

Although ion chemistry models[1,2] have predicted proton hydrates (PH) that is ions of the form $H^+(H_2O)_n$, as major ions in the stratosphere, the first *in situ* mass spectrometric measurements[3–5] revealed another ion family, called non-proton hydrates (NPH). The fractional abundance of these NPH, represented by $H^+X_l(H_2O)_m$, increases from 1 to 90% between 55 and 23 km (refs 1, 5–7). Several proposals[5,8,9] have been made for the identity of the molecule X, but high resolution spectra[10] and ion abundance measurements[11,12] suggest that X should be acetonitrile (CH_3CN). This suggestion has been reinforced by laboratory measurements[13,14] and *in situ* data between 20 and 42 km (refs 6, 7), allowing a determination of the concentration profile of X in this altitude region. Here we report the first positive ion composition data obtained using a balloon-borne instrument between 42 and 46 km altitude. These data extend the density profile of X and give supplementary indications about its identity.

The data were obtained with a mass spectrometer that was flown on 23 September 1982 on a 1,000,000 m^3 stratospheric balloon from the CNES launching base of Aire-sur-l'Adour (44° N). Also included in the payload, and mounted above the mass spectrometer, were: a gondola containing photographic equipment for the detection of aerosol layers and an instrument for measuring ozone by means of UV absorption.

The instrument was launched at 12.38 UT and the flight lasted about 7 h. A float altitude of 46 km was reached at 16.00 UT and after sunset the balloon descended slowly to 42 km. The altitude was determined independently from a pressure measurement using a high-precision Baratron gauge and from high resolution radar tracking. The difference between both results was 300 m. Spectra of positive as well as negative ions have been obtained from 46 to 42 km. The negative ion composition data will be reported elsewhere.

The instrument used to obtain the spectra consists of a microprocessor-controlled quadrupole ion mass spectrometer with a mass range of 10–330 AMU and is essentially the same as one that has been described in detail elsewhere[10,15]. To obtain a greater sensitivity at high altitudes, a larger ion sampling hole (0.4 mm diameter) was used.

Because no major ion groups other than PH and NPH were detected, all positive ion spectra used here were recorded in a moderate resolution mode ($m/\Delta m \cong 17$) that was sufficient to resolve the major ions and their fractional abundance. At some times spectra were recorded in the total ion mode (no d.c. on the quadrupole rods) or with low resolution, which allowed an estimation of the abundance of ions having a mass larger than 256 AMU (ref. 7). To minimize the possible effects of contamination[7], all useful data were recorded either at float altitude or during the descent part of the flight, with the ion sampling hole pointing downwards.

A typical positive ion spectrum obtained at float altitude is shown in Fig. 1. All major mass peaks below 150 AMU can be attributed to either PH ions (masses 55, 73 and 91) or NPH clusters (masses 78, 96,. . .). Two groups of mass peaks are also present around 278 and 310 AMU. The intensity of these peaks fluctuated with altitude and increased during ascending phases of the balloon altitude oscillations. In spectra recorded during the descent of the balloon, these mass peaks due to contamination were much less pronounced. Laboratory studies in our institute have shown that these ions originated from gases desorbing from the painted surfaces of the photographic payload, heated by solar radiation. These gases appeared to be mainly dibutylphthalate and butylbenzylphthalate vapours; two solvents present in the paint.

As has already been pointed out[5], the number density of X can be calculated from the observed fractional ion abundances through the continuity equation for NPH:

$$k_1[\mathrm{PH}][\mathrm{X}] = \alpha[n_-][\mathrm{NPH}] \quad (1)$$

where α is the ion–ion recombination coefficient, $[n_-]$ the total negative ion density and k_1 the rate coefficient for the reactions of the type

$$H^+(H_2O)_n + X \rightarrow H^+X(H_2O)_{n-1} + H_2O \quad (2)$$

The total fractional abundances of NPH ions and PH ions, [NPH] and [PH], can be deduced from the ion mass spectra, assuming that ion count rates are reflecting ion abundances. This assumption is believed to be acceptable in view of the moderate resolution used, resulting in low mass discrimination effects.

For k_1 a value of 3×10^{-9} $cm^3\,s^{-1}$ was chosen, according to the laboratory measurements of Smith and colleagues[14]. The $[n_-]$ was calculated with the parametrization formula of Heaps[16].

For α a parametrization of the form

$$\alpha = 6\times10^{-8}\left(\frac{300}{T}\right)^{1/2} + 1.25\times10^{-25}[\mathrm{M}]\left(\frac{300}{T}\right)^{4} \ \mathrm{cm^3\,s^{-1}} \quad (3)$$

was adopted where T is the temperature in Kelvin and [M] the total neutral number density in cm^{-3}. This is a compromise for the different values of α as obtained by recent *in situ* measurements[17], laboratory experiments[18] and theoretical studies[19].

The concentrations of X, thus obtained from spectra similar to Fig. 1 are converted to mixing ratios and represented in Fig. 2 for the different altitudes covered by the present flight.

In the above derivations of [X] using the continuity equation (1), it was assumed that the contaminant gases giving rise to heavy ions (around mass 278 and 310 AMU) do not affect the ambient ion chemistry. To investigate the possible role of contamination in our calculations, we will represent the real number density of X by

$$[\mathrm{X}]_R = [\mathrm{X}](1+\varepsilon) \quad (4)$$

where [X] is the number density inferred from equation (1). The relative error ε will now be calculated for two extreme reaction schemes, which could modify the simple ion chemistry leading to equation (1). In the first one we assumed that the contaminants react with both PH and NPH and give rise to heavy ions CI, which subsequently disappear by recombination. Considering the continuity equation for NPH and CI leads to:

$$\varepsilon = k_3[\mathrm{CI}](k_2[\mathrm{PH}] + k_3[\mathrm{NPH}])^{-1} \quad (5)$$

where k_2 and k_3 are common rate constants for the reactions of contaminants with PH and NPH respectively. This implies that the values of [X] would be too low by a factor $(1+\varepsilon)$. The relative error ε reduces to zero if the contaminants react with PH only ($k_3 = 0$). When $k_2 \cong k_3$ the error ε is estimated to be at maximum 1 in the most contaminated spectra, used for the derivation of [X]. This is concluded from estimations of [CI]/([PH]+[NPH]) in spectra obtained at very low resolution or in the total ion mode, where few or no errors are induced due to the limited mass range of the instrument. When the

0028–0836/83/210314—03$01.00

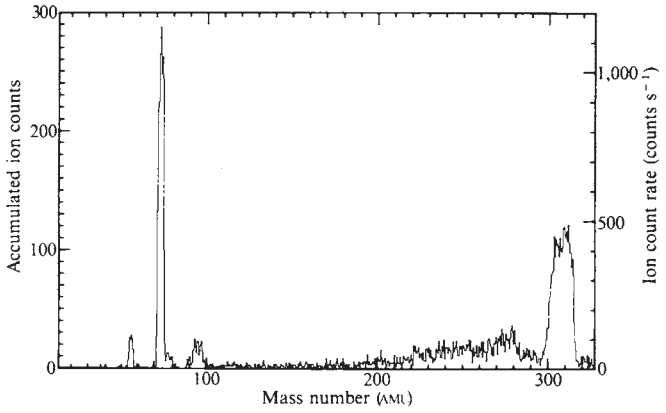

Fig. 1 Typical positive ion spectrum obtained around 45.6 km altitude in the moderate resolution mode ($m/\Delta m \cong 17$). The spectrum has been obtained after 1 scan of 160 s for the mass domain 10–330 AMU. This spectrum has been chosen to show clearly the presence of contaminant ions (mass 278 and 310 AMU). The first part of this spectrum was obtained during a descending phase of the balloon excursion whereas the second half was recorded during ascent.

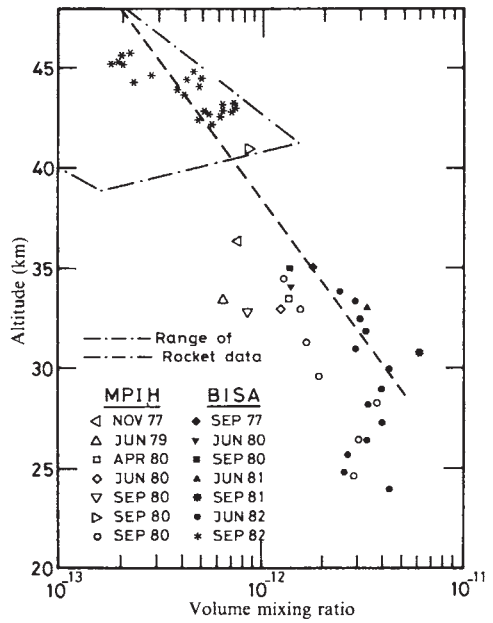

Fig. 2 Volume mixing ratio of X as calculated from ion abundances. Data MPIH were obtained by the group of the Max-Planck-Institut of Heidelberg[5,6,11]. Data BISA are from Belgian Institute for Space Aeronomy[4,7,10]. The range of rocket data, obtained by Arnold and colleagues[2] has been taken from a compilation by Henschen and Arnold[6]. The dotted straight line represents an approximation of the form $f(CH_3CN) = 6\times10^{-10}\exp(-z/6)$, with z in km.

contaminants are reacting with NPH only ($k_2 = 0$), ε can become very large. This would mean that for high values of [CI] lower values of [X] should be found. However, spectra obtained during ascending phases of the balloon and showing high [CI] values seem to indicate the opposite (these spectra were not used for [X] derivations). This leads us to believe that the first proposed reaction scheme is unlikely.

Another modification of the continuity equation for NPH arises when the contaminant gases react with PH and the resulting CI subsequently react with X to form extra NPH. Continuity considerations now result in:

$$\varepsilon = -k_4[\mathrm{CI}]\,(k_1[\mathrm{PH}]+k_4[\mathrm{CI}])^{-1} \qquad (6)$$

where k_4 is the reaction rate coefficient of X with CI. Assuming $k_1 \cong k_4$ (which is an extreme case, in view of the large value of k_1) the values of [X] should be reduced by a factor of 2 in the worst case of contamination for the spectra used, when [CI] ≅ [PH].

As a general conclusion we feel that it is safe to accept an error of a factor of 2 due to contamination for the values of [X] as derived in this work. In fact below 44 km where the balloon descended at a rate of 1.3 m s^{-1}, we believe that this error is much smaller, due to the lower outgassing of the optical payload after sunset and due to the induced air flow. This is also confirmed by a total ion mode spectrum, obtained below 44 km during descent, which shows a total abundance of [CI] $<10\%$. Furthermore the reasonable agreement of our data points with the rocket data, as observed in Fig. 2, strengthens our faith in their reliability.

Considering the previous remarks and the uncertainty on the quantities α, k_1 and $[n_-]$ used in equation (1), the maximum total error on the data is estimated to be a factor of 3.

When combined with results of previous balloon flights a more complete mixing ratio profile of the molecule X is now obtained. This profile, showing a slow decrease of the mixing ratio of X above 30 km, suggests[6,7] a source of X below 30 km.

If X were CH_3CN such a source might be surface production by industrial releases or biomass burning (P. Crutzen, personal communication), followed by wash-out, diffusion and photochemical destruction. Recent observations by Becker and Ionescu[20] indicate that the concentration of CH_3CN at ground level ranges from 2 to 7 parts per 10^9 by volume, which support the hypothesis of surface emission, followed by strong heterogeneous removal.

For CH_3CN, the emission factors of which are not known yet, the loss processes one expects are reaction with OH and photodissociation. Since, however, light absorption by CH_3CN and resulting photolysis only start in the far UV (refs 21, 22), the main loss happens through reaction with the hydroxyl radical. Reactions with $O(^1D)$ and Cl may also contribute to the destruction of CH_3CN, although due to the low concentrations of these species and the expected slower reactions this loss term can probably be neglected here. In such a case the steady state continuity equation for CH_3CN can be simplified to

$$\frac{\partial\phi(\mathrm{CH_3CN})}{\partial z} + k[\mathrm{OH}]\,[\mathrm{M}]\,f(\mathrm{CH_3CN}) = 0 \qquad (7)$$

with

$$\phi(\mathrm{CH_3CN}) = -K[\mathrm{M}]\frac{\partial f(\mathrm{CH_3CN})}{\partial z} \qquad (8)$$

where [OH] is the number density of hydroxyl radicals, k the reaction rate coefficient of CH_3CN with OH, $f(CH_3CN)$ the mixing ratio and K the eddy diffusion coefficient.

The reaction rate coefficient k, as measured by Harris *et al.*[23], is given by

$$k = 5.86\times10^{-13}\exp(-750/T) \quad \mathrm{cm^3\,s^{-1}} \qquad (9)$$

The total density [M] can be easily calculated from the ideal gas law and the US Standard Atmosphere. If then we take according to Brasseur *et al.*[24]

$$K = 1{,}019\exp(z/9.43) \quad \mathrm{cm^2\,s^{-1}} \qquad (10)$$

(z in kilometres), and approximate the mixing ratio $f(CH_3CN)$ in the altitude region 33–45 km by

$$f = 6\times10^{-10}\exp(-z/6) \qquad (11)$$

which is the dotted straight line in Fig. 2, the equations (7) and (8) can be solved analytically and the OH mixing ratio can be calculated from the approximated CH_3CN profile.

The result of such a calculation is shown in Fig. 3 for US Standard Atmosphere, autumn temperature conditions. The

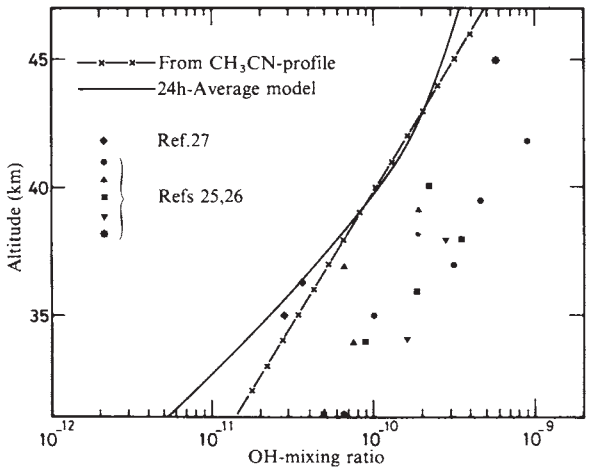

Fig. 3 OH volume mixing ratio profile calculated assuming that X were CH_3CN, and compared with measurements and model calculations. Data for 24-h average model from G. Brasseur (personal communication).

obtained OH profile is compared with recent measurements, performed by different authors[25–27].

As can be seen the OH mixing ratios of this work are considerably lower than the measurements. Note, however, that the measurements represent instantaneous values of [OH], whereas the data calculated here are 24 h averages, taking into account the long lifetime of CH_3CN versus the OH reactions (between 400 and 1,000 h for the altitude region under consideration).

In fact, a comparison of the OH profile calculated from the CH_3CN profile with a recent model calculation of the 24-h average of OH according to G. Brasseur (personal communication) turns out to be quite satisfactory, in view of the simple CH_3CN profile assumed (a straight line on semi-log plot). The reasonable agreement of these OH data with previous work can be considered as additional evidence for the identification of X as CH_3CN.

A more complete model of CH_3CN, taking into account possible surface sources, washout in the troposphere, diffusion and photochemical destruction is clearly needed to elucidate this problem. At present, however, the available data seem to indicate that the molecule X is indeed CH_3CN.

We thank the technical staffs of the Belgian Institute for Space Aeronomy and the CNES launching base at Aire-sur-l'Adour which made the experiments possible; also Dr Vrignault and the technical staff of the Centre d'Essais des Landes for the radar tracking during the balloon flight and Dr M. Ackerman for organizing the joint flight. Part of this project was financed by the NFWO (Belgian National Science Foundation) as project no. 2.0009.79.

Received 24 January; accepted 22 March 1983.

1. Mohnen, V. A. *Pure appl. Geophys.* **84,** 114–153 (1971).
2. Ferguson, E. E. in *Natural Stratosphere of 1974* (CIAP Monogr. 1, 5.42–5.54, 1974).
3. Arnold, F., Krankowsky, D. & Marien, K. H. *Nature* **267,** 30–32 (1977).
4. Arijs, E., Ingels, J. & Nevejans, D. *Nature* **271,** 642–644 (1978).
5. Arnold, F., Bohringer, H. & Henschen, G. *Geophys. Res. Lett.* **5,** 653–656 (1978).
6. Henschen, G. & Arnold, F. *Geophys. Res. Lett.* **8,** 999–1001 (1981).
7. Arijs, E., Nevejans, D., Ingels, J. & Frederick, P. *Annales Geophysicae* **1,** 163–168 (1983).
8. Ferguson, E. E. *Geophys. Res. Lett.* **5,** 1035–1038 (1978).
9. Murad, E. & Swider, W. *Geophys. Res. Lett.* **6,** 929–932 (1979).
10. Arijs, E., Nevejans, D. & Ingels, J. *Nature* **288,** 684–686 (1980).
11. Arnold, F., Henschen, G. & Ferguson, E. E. *Planet. Space Sci.* **29,** 185–193 (1981).
12. Arijs, E., Nevejans, D. & Ingels, J. *J. atmos. terr. Phys.* **44,** 681–694 (1982).
13. Bohringer, H. & Arnold, F. *Nature* **290,** 321–322 (1981).
14. Smith, D., Adams, N. G. & Alge, E. *Planet. Space Sci.* **4,** 449–454 (1981).
15. Ingels, J., Arijs, E., Nevejans, D., Forth, H. J. & Schaefer, G. *Rev. scient. Instrum.* **49,** 782–784 (1978).
16. Heaps, M. G. *Planet. Space Sci.* **26,** 513–517 (1978).
17. Rosen, J. M. & Hofman, D. J. *J. Geophys. Res.* **86,** 7406–7420 (1981).
18. Smith, D. & Adams, N. G. *Geophys. Res. Lett.* **9,** 1085–1087 (1982).
19. Bates, D. R. *Planet. Space Sci.* **30,** 1275–1282 (1982).
20. Becker, K. M. & Ionescu, A. *Geophys. Res. Lett.* **9,** 1349–1351 (1982).
21. Herzberg, G. & Scheibe, G. *Z. phys. Chem.* **B7,** 390–394 (1930).
22. McElcheran, D. E., Wynen, M. H. J. & Steacie, D. W. R. *Can. J. Chem.* **36,** 321–329 (1958).
23. Harris, G. W., Kleindienst, T. E. & Pitts, J. N. *Chem. phys. Lett.* **80,** 479–483 (1981).
24. Brasseur, G., De Rudder A. & Roucour, A. in *Proc. int. Conf. Environmental Pollution*, Thessaloniki, 839–910 (1982).
25. Anderson, J. G. *Geophys. Res. Lett.* **3,** 165–168 (1976).
26. Anderson, J. G. in *Proc. NATO Advances Study Institute on Atmospheric Ozone*, FAA-EE-80-20, 253–251 (1981).
27. Heaps, W. S. & McGee, T. J. *J. geophys. Res.* (submitted); *The Stratosphere 1981, Theory and Measurements*, 1–105 (WMO Rep. No. 11, 1981).

Direct surface imaging in small metal particles

L. D. Marks

Cavendish Laboratory, Madingley Road, Cambridge CB3 0HE, UK

David J. Smith

High Resolution Electron Microscope, University of Cambridge, Free School Lane, Cambridge CB2 3RQ, UK

Atomic-level information about the surfaces of small metal particles has been recorded directly in recent observations with a 600-kV high-resolution electron microscope. Here, we have studied small polycrystalline particles of silver and gold tilted to bring their surfaces parallel to the electron beam. However, unlike previous workers using this normal reflection electron microscopy (REM) configuration, we have used conventional bright field axial imaging thereby considerably facilitating image interpretation. As well as clean, sharp surface images, morphological details of catalytic significance, such as the distribution of surface steps, particle facetting and the nature of surface reconstructions, have been obtained. Moreover, detailed computer simulations confirmed that the electron micrographs can be interpreted in terms of atomic columns and, in particular, established that some micrographs showed, for the first time in a transmission electron microscope (TEM), direct atomic-scale imaging of a reconstructed metal surface.

The first direct atomic imaging in the electron microscope was achieved by Crewe and co-workers using the scanning transmission instrument[1], and several workers[2,3], have demonstrated that imaging of atoms is feasible, although less straightforward, in the conventional TEM using tilted-beam dark-field illumination. Good quantitative agreement between experimental bright-field images of isolated tungsten atoms and clusters with calculated contrast levels has also been obtained[4]. Furthermore, it is possible to obtain images of crystals showing surface information on the atomic scale. For example, surface steps in projection have been observed[5] in MgO and gold[6] in weak-beam dark-field imaging conditions and also in gold[7] using forbidden reflections, whilst single atomic steps on the (111) surface of silicon crystals were imaged using a bright field technique[8]. Cowley has used the scanning TEM in a glancing incidence surface imaging mode[9] to observe unit-cell-high steps on the faces of MgO crystals. This REM technique, which utilizes electrons incident at glancing angles (and thereby produces a severely foreshortened image) has also been used to good effect in TEM studies of surface topography. Direct observations, for example, of superstructures in silicon resulting from surface reconstruction have been made[10]. The various configurations and results for surface imaging have been recently reviewed[11].

The specimens of silver and gold were prepared by evaporation and epitaxial growth on heated alkali halide substrates, as described elsewhere[12]. These were examined at either 500 or 575 kV using the Cambridge University high-resolution electron microscope (HREM)[13]; recent modifications and increased resolution[14] have resulted in almost an order of magnitude improvement in the signal-to-noise ratios for the common lattice spacings (0.235 nm for 111 beams and 0.204 nm for 200) and experimental imaging conditions could be accurately chosen by direct particle observation using an image pick-up

0028-0836/83/210316—02$01.00